

https://dspace.org/

Fracture Mechanics Analyses Of Static And Dynamic Failures Associated With Welding

Boothroyd, Colin Allistair

2015-01-09
http://hdl.handle.net/10539/16336

Downloaded from a DSpace repository. https://dspace.org/

reflected in Figures 3.9, 3.10 and 3.11 where the significant variation in defect parameters causes only a slight effect on the failure stress levels). It must be pointed out that the effective defect parameter (a) and the failure strain ratio were more markedly affected by the variation in the input data.

Figures 3.9, 3.10 and 3.11 also give an indicatior of the weld metal "defect tolerance". Clearly, fracture mechanics assessments of the weld metal which records the greatest change in failure stress due to the variation of the defect parameters will be most affected by inaccuracies in UT defect sizing. For the four weld metals under consideration, the stress-relieved MMA material was most affected by variations in defect height and ligament. It will be seen from Table 3.1 that this material had the highest yield stress and lowest CTOD toughness of the four weld metals, and this would tend to indicate that it is in fact the least defect tolerant. However, the stress-relieved MMA material was the least affected by defect length variations. It is considered that this is a result of the low ultimate tensile strength to yield stress ratio of this material, and therefore, for a given range of failure strain ratios, all greater than unity, this material will record the lowest variation in failure stress levels.

Figure 3.12 shows the variation in failure stress with increasing CTOD toughness, for the reference defect of 10 mm in height, 50 mm in length, with a tensile ligament of 5 mm. As outlined earlier, varying the CTOD toughness while maintaining a constant stress-strain behaviour may not be strictly valid. However, this graph does show that, for this particular situation, there is a critical value of CTOD toughness above which the failure stress does not vary significantly. This point of inflexion corresponds to the point at which the failure strain ratio becomes greater than unity, and the failure stress will not be significantly affected by variations in the failure strain ratio. For the four weld metals under consideration, this "critical" CTOD was between 0,07 and 0,08 mm, and less than both the initiation CTOD and the maximum CTOD for these weld metals. For a different defect size (or a different material), it is

feasible that the point of inflexion in this graph may lie between the initiation CTOD and the CTOD at maximum load. Obviously, in such a situation, the choice of CTOD toughness to be used is crucial to the accuracy of the assessment.

3.3.2 The CEGB R-6 Failure Assessment Diagram.

As described earlier in Section 3.1.4, this approach requires that two parameters be calculated, an elastic parameter, K_r and a plastic parameter, S_r. K_r is the ratio of the stress intensity (K_I) calculated for the assumed flaw and applied load, to the material plane strain fracture toughness, K_{Ic}; S_r is the ratio of the applied load to that load required to cause plastic collapse of the defective section. In this work, the plane strain fracture toughness was estimated using the regression technique contained in an Appendix to the R-6 document, and the plastic collapse load was calculated as outlined earlier in Section 3.2.2.

Figures 3.13, 3.14 and 3.15 show the effect of varying the defect parameters of height, critical ligament and length respectively. Thus, in the first instance, Figure 3.13 shows that the defect height reaches a limiting value, above which the S_r parameter remains constant. This is due to the through-thickness stress distribution, which indicates that once the top of the defect lies above the neutral axis position, it experiences compressive stresses (which it can support) and thus the load required for plastic collapse remains constant. Figure 3.14 shows that the method used for calculating the plastic collapse load is sensitive to changes in defect depth, and hence to the extent of the critical ligament. In Figure 3.15 it can be seen that results appearing on the R-6 Failure Assessment Diagram are also influenced by increasing the defect length, and that this has the effect of increasing defect criticality.

It would appear from these three Figures that, for a given defect size and depth, the stress-relieved MMA material is the most defect tolerant. This is

most evident in Figure 3.13, where the locus of the points defined by the S_r and K_r parameters calculated for the defect heights ranging between 1 and 20 mm is contained within the non-critical region of the failure assessment diagram.

Interestingly, this result would seem to be at variance with the results obtained using the PD 6493 Design Curve route, and there appear to be two main reasons for this apparent anomaly:-

(a) there is no recategorisation of embedded defects to surface defects in the R-6 approach;

(b) the stress-relieved MMA weld metal had the highest flow stress so that for a given defect size, this material will have the highest plastic collapse load, and the lowest S_r parameter.

With regard to the former, it can be seen in Figures 3.9 and 3.10 that, for the embedded defects (ie. if plastic collapse does not occur), the stress-relieved MMA weld metal gave the highest failure stress level, for a given defect size. This indicates that there is some compatibility in the two assessment procedures.

3.4 Summary

This Chapter has reviewed the various failure modes, and how current design philosophies can be used to prevent these. Two widely applied failure assessment procedures, BS PD 6493, and the CEGB R-6 document, were discussed, with special reference to brittle fracture. It was shown that there could be some uncertainty when predicting failure stresses from the Design Curve in PD 6493 at high applied strains; and that the R-6 method requires the user to perform a sensitivity analysis to establish, more precisely, the safety margins in any assessment of defect criticality, using the Failure Assessment Diagram.

The results obtained in this sensitivity analyses, performed for both assessment procedures, have indicated that the proposed method of calculating failure stress levels and defect criticalities are indeed sensitive to variations in the input data. They can therefore be used with confidence in assessing the effect of ultrasonic defect detection variability on fracture mechanics assessments of these particular defective welds tested under bending loads. The results of this assessment will be detailed in Chapter Five, to follow.

Additionally, this type of sensitivity analysis can be used much more widely to determine the relative defect tolerance of different weld metals, under some pre-defined set of operating conditions. This could have particular value for optimising material selection in the fabrication industry, and would also indicate whether or not a heat treatment stress-relief would beneficially affect the defect tolerance of a given component or structure.

TABLE 3.1 : Summary of weld metal mechanical and fracture properties.

	MMA1	SA1	MMA2	SA2
CTOD d_{max} (mm)	0,20	0,23	0,14	0,22
K_c(MPa $\sqrt{m}$)	120	139	110	126
Yield stress (MPa)	580	623	666	599
Tensile strength (MPa)	683	699	744	704
Flow stress (MPa)	632	661	705	652
Yield strain ($x10^{-3}$)	2,83	3,04	3,25	2,92

Note

(1) The suffixes 1 and 2 refer to the as-welded and stress-relieved conditions respectively.

(2) Specimen thicknesses were not sufficient for a valid K_{Ic}, and thus only a K_c is reported.

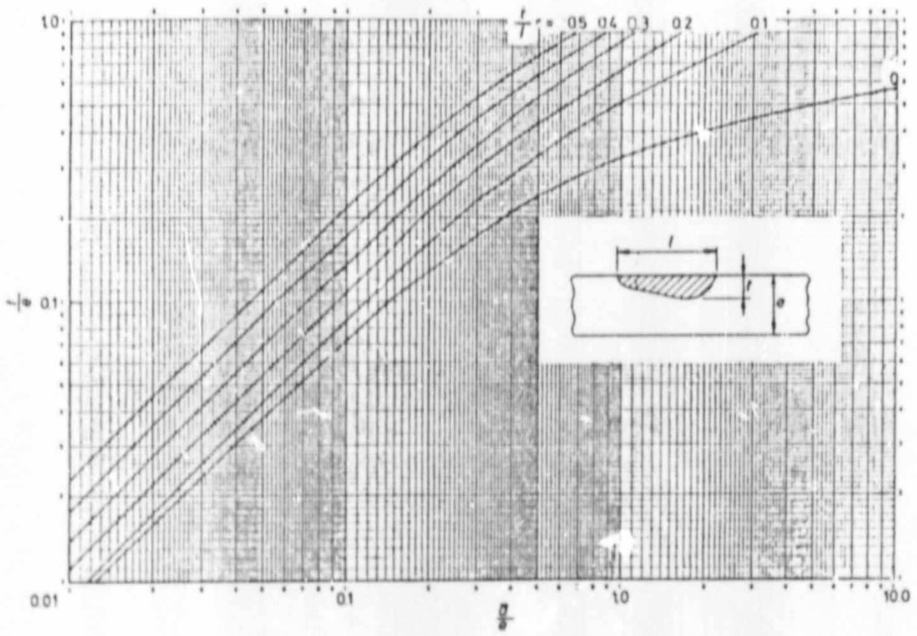

Figure 3.1 Graphical solution for the effective defect parameter of a surface defect (reproduced from PD 6493 (3)).

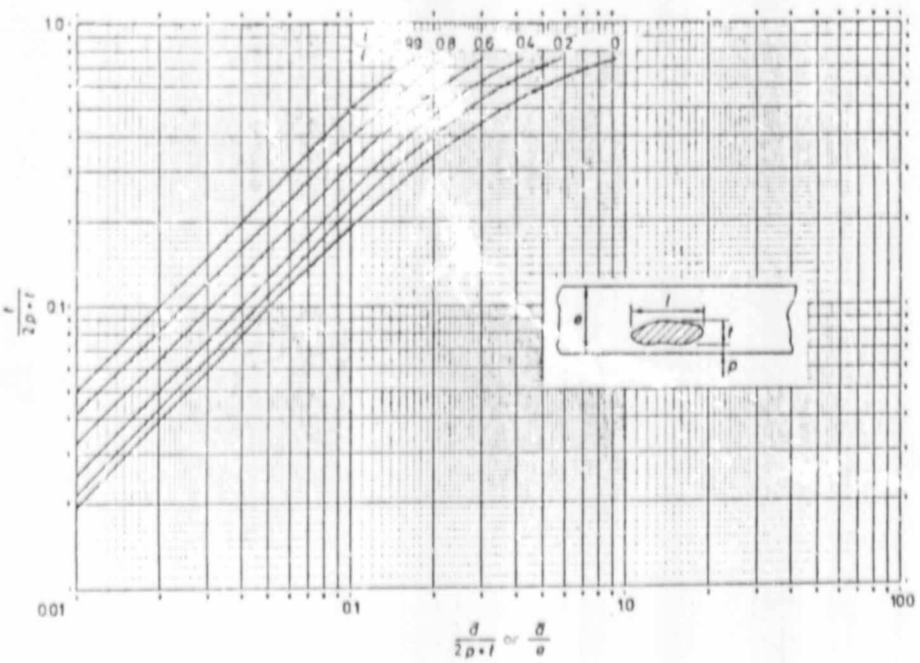

Figure 3.2 Graphical solution for the effective defect parameter of an embedded defect (reproduced from PD 6493 (3)).

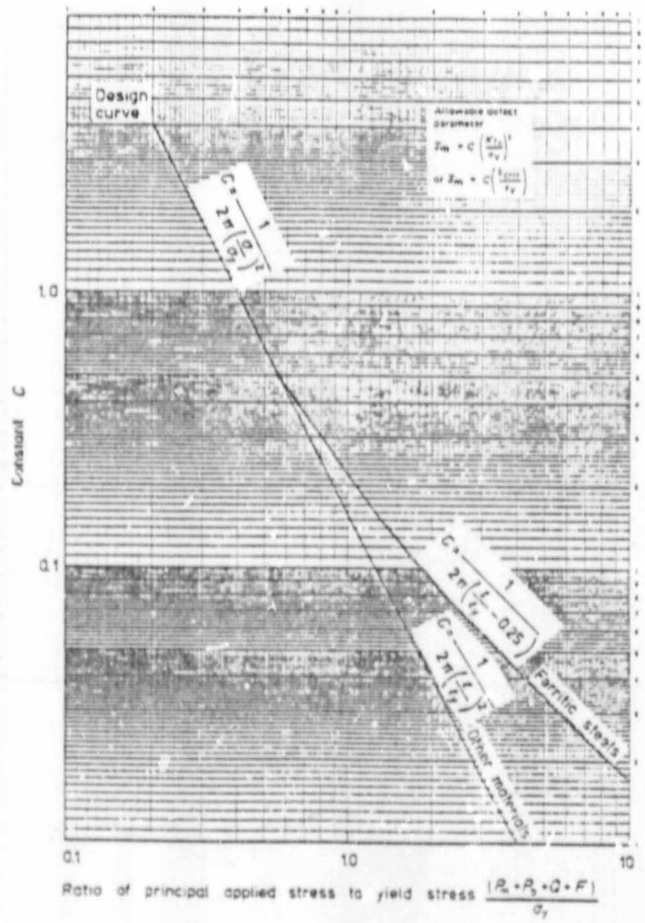

Figure 3.3 The Design Curve in PD 6493 (3) which gives values of the constant C for different loading conditions or defect sizes.

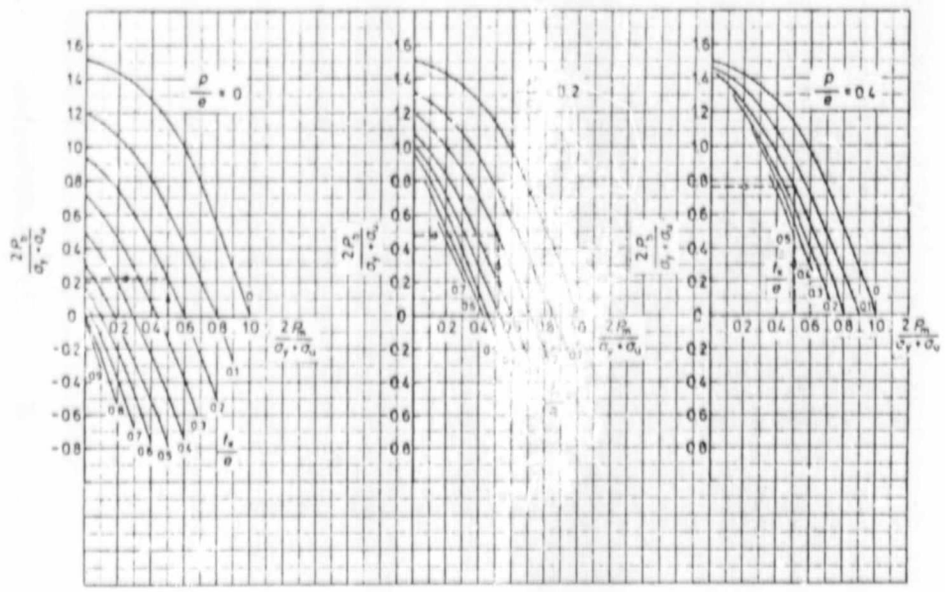

Figure 3.4 The graphical recategorisation procedure to check for ligament stability of embedded defects (from PD 6493 (3)).

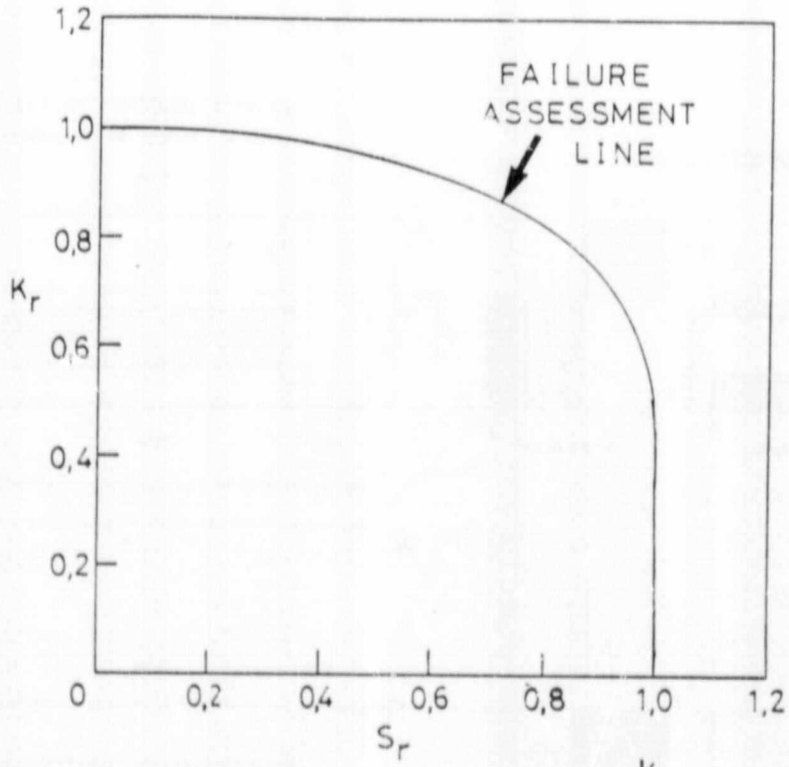

$$K_r = S_r \left[\frac{8}{\pi^2} \ln \sec\left(\frac{\pi}{2} S_r \right) \right]^{-\frac{1}{2}}$$

Figure 3.5 The CEGB R-6 Failure Assessment Diagram to check for defect criticality (from (4)).

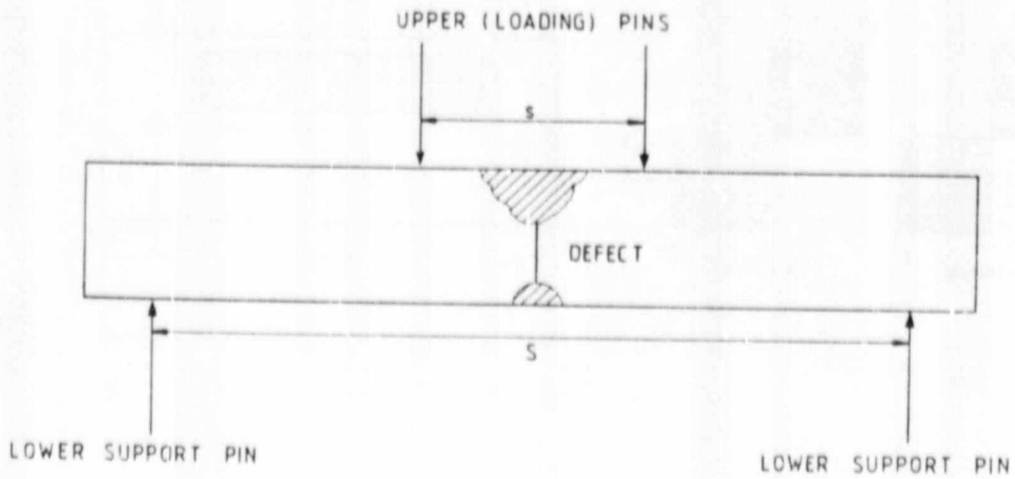

$$\text{MOMENT ARM} = \frac{S - s}{2}$$

Figure 3.6 A schematic of the four point bend configuration.

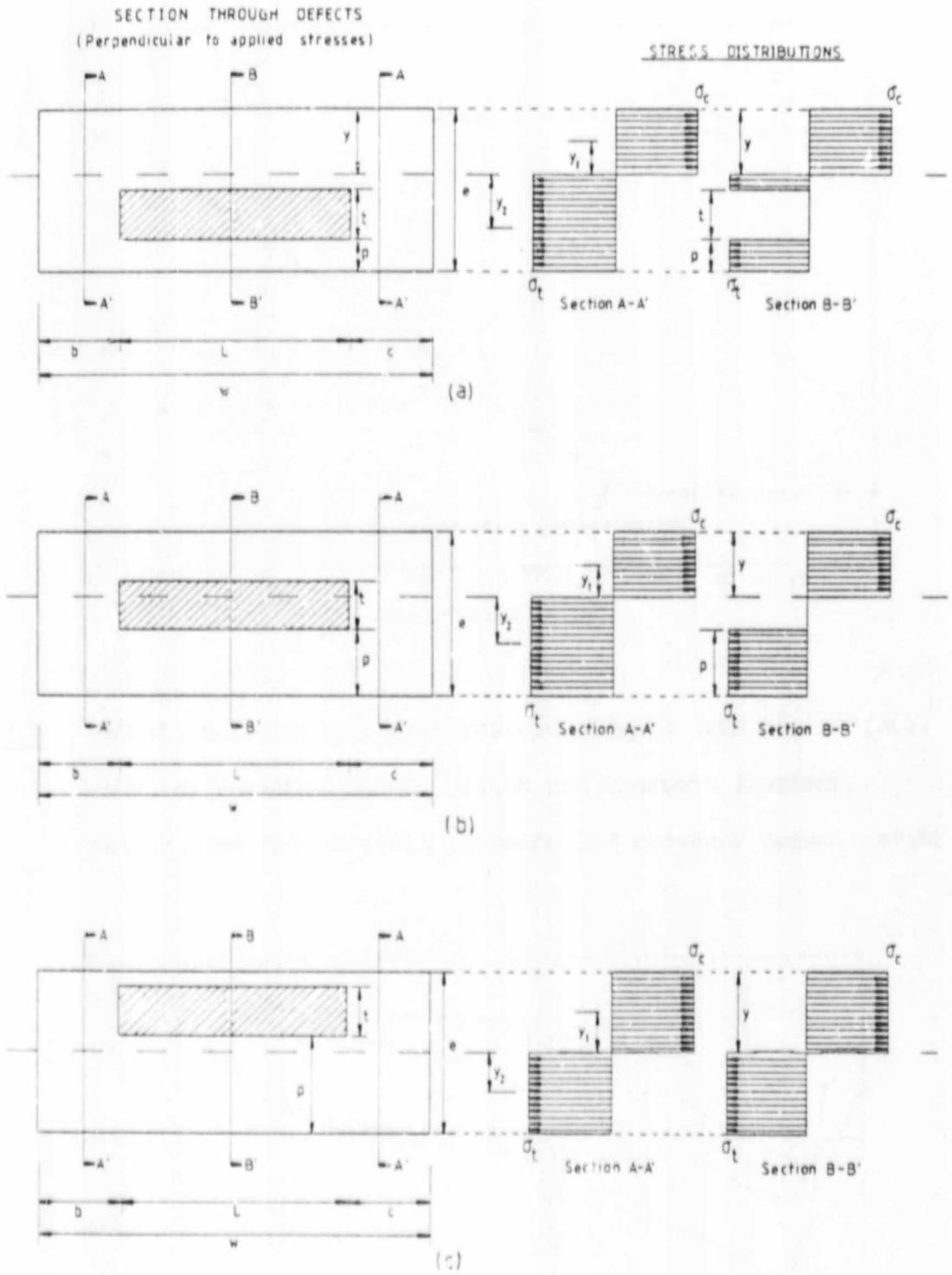

Figure 3.7 The assumed stress distributions for the three defect positions relative to the neutral axis (a) defect below the neutral axis in the tensile region, (b) the neutral axis intersects the defect at some point, and (c) the defect is above the neutral axis, in the compressive region, and the defective weld acts as a homogeneous beam.

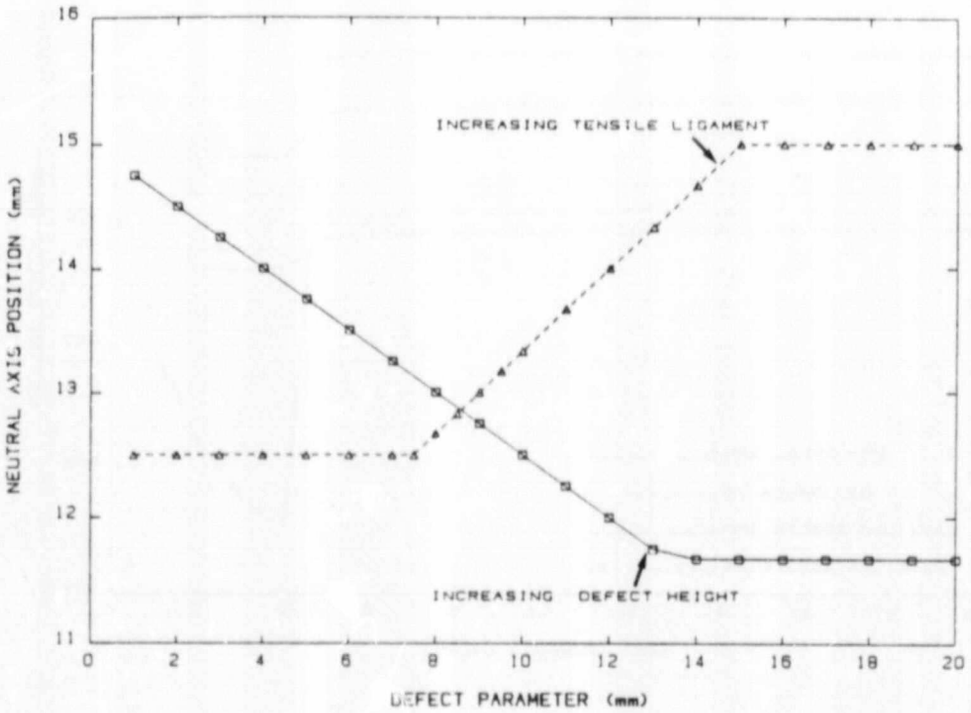

Figure 3.8 Variation in neutral axis position (depth from top surface) with (a) variable defect height and constant ligament length, and (b) variable ligament and constant defect height.

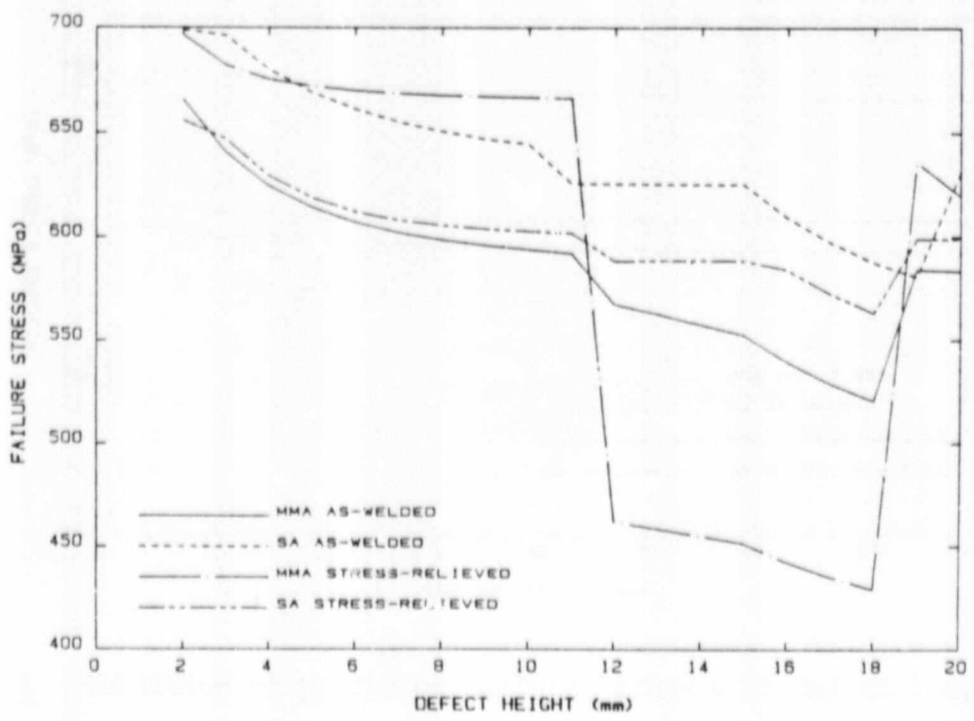

Figure 3.9 Variation in predicted failure stress with defect height (defect length and ligament constant).

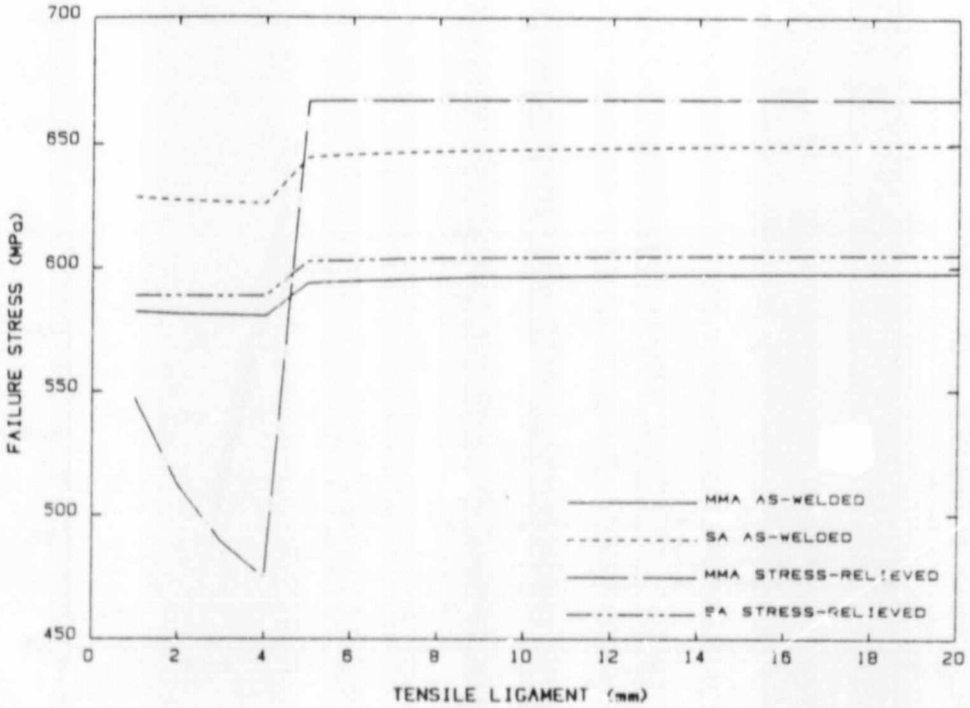

Figure 3.10 Variation of predicted failure stress with critical ligament (defect height and length constant).

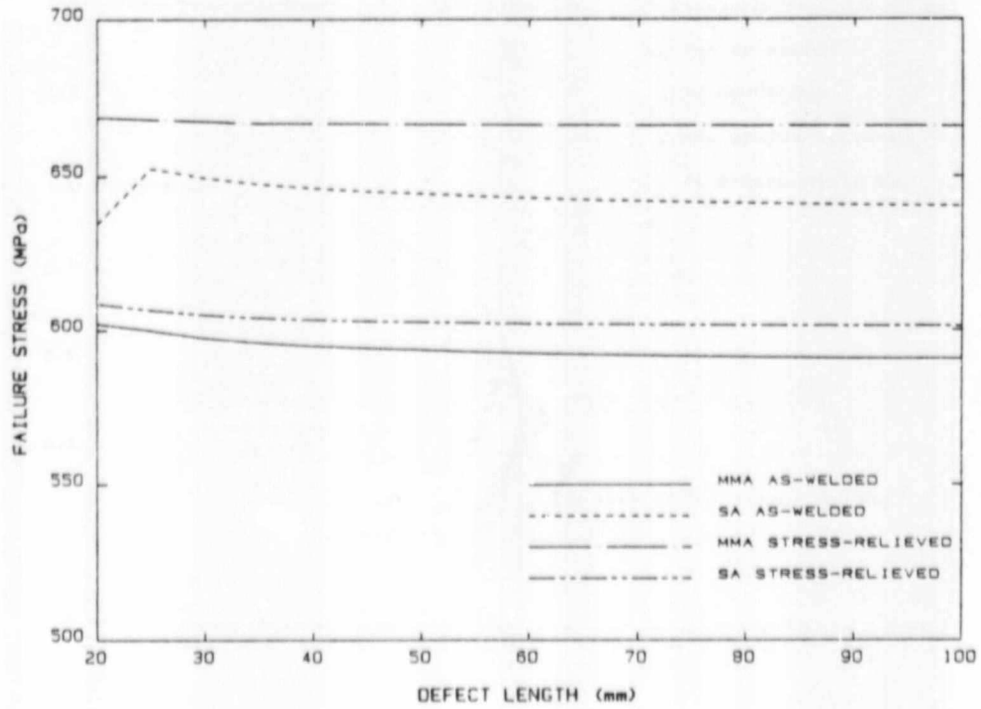

Figure 3.11 Variation of predicted failure stress with defect length (defect height and ligament constant).

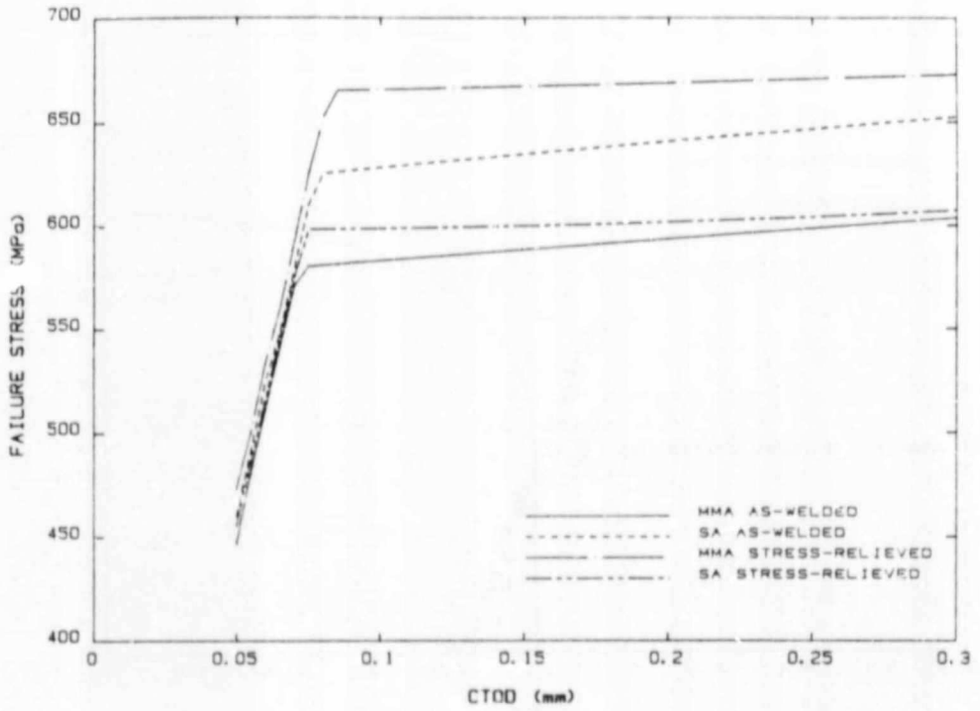

Figure 3.12 Variation of predicted failure stress with CTOD toughness. (Constant defect size and position).

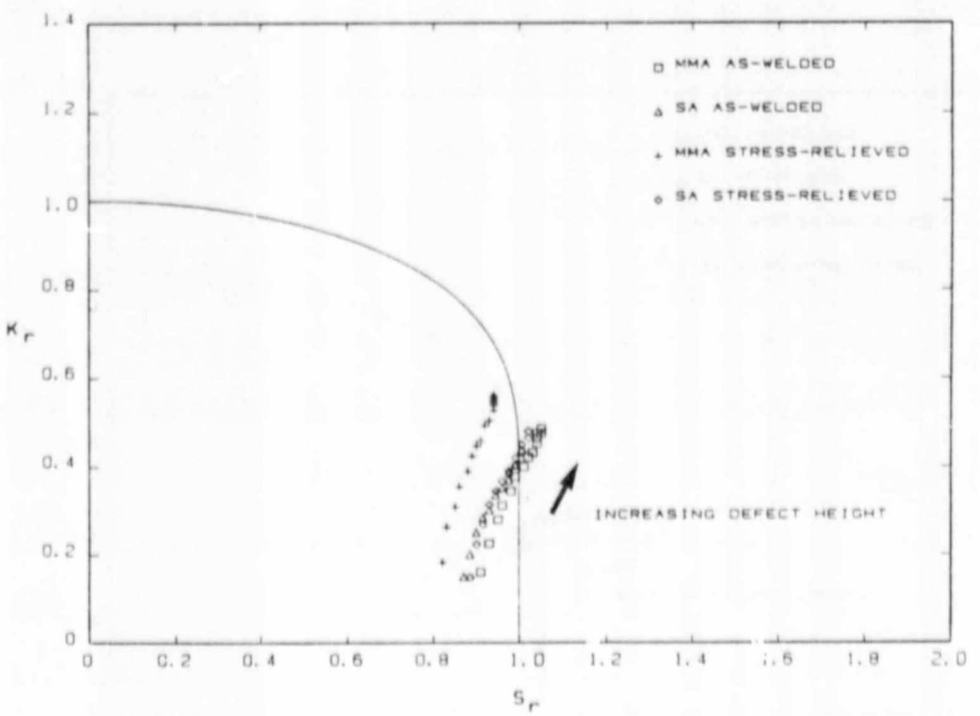

Figure 3.13 Effect of increasing defect height over the range 1 to 20 mm on the failure assessment diagram (with defect length fixed at 50 mm and critical ligament fixed at 5 mm).

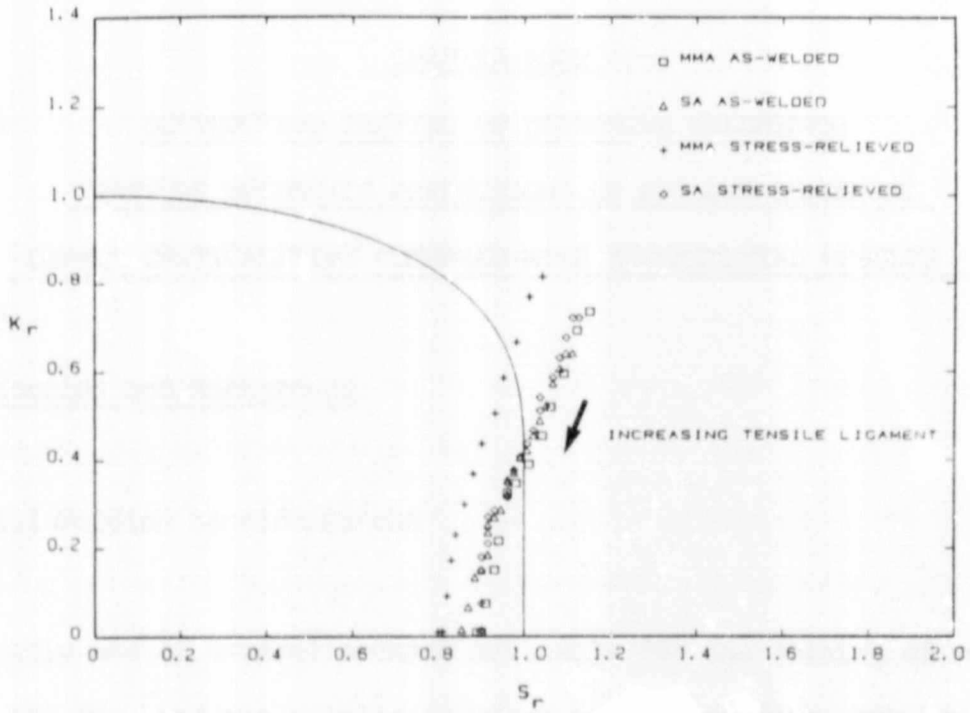

Figure 3.14 Effect of decreasing critical li ament ngth over the range 20 to 1 mm on the failure assessment diagram (defect length fixed at 50 mm and defect height fixed at 10mm).

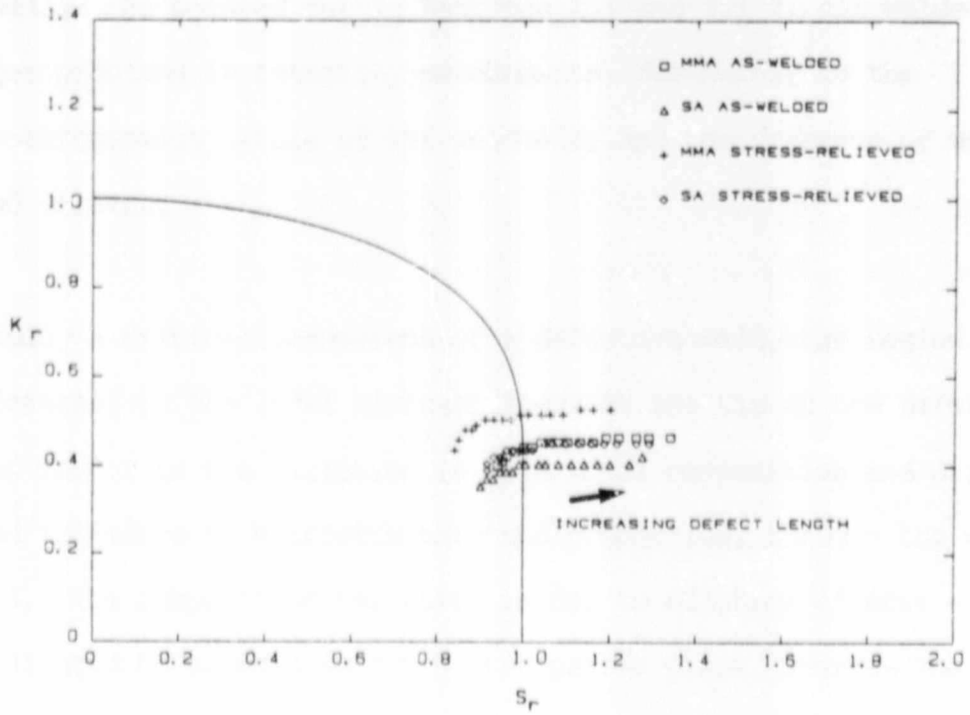

Figure 3.15 Effect of increasing defect length over the range 20 to 100 mm on the failure assessment diagram (defect height fixed at 10 mm and critical ligament fixed at 5 mm).

CHAPTER FOUR

DESTRUCTIVE TESTING OF DEFECTIVE WELDMENTS: FRACTURE MECHANICS PREDICTIONS OF FAILURE LOADS AND DEFECT CRITICALITIES COMPARED WITH EXPERIMENTAL RESULTS

4.1 Introduction and Background

4.1.1 Welding considerations

Welding is only one of several methods available for the joining of metallic components (69,70), and the problem is often not how to join, but how to select the best method. Fusion welding processes, such as gas welding, arc welding and resistance welding have essentially replaced rivetting for the joining of steel sections and plate. However, common weld designs often introduce geometries that are effective cracks, or at least, likely crack initiation sites, albeit unintentionally. As pointed out in Sections 1.1 and 3.1.2, all-welded designs present major problems in integrity assessments, due mainly to the structure-heterogeneous nature of the weldment, and the presence of weld induced stresses and strains.

When performing a critical assessment of a defective weld, the region of principal interest is the local microstructure at the tip of the defect. A complicating factor is the variation in weld metal composition and prior thermal history, and therefore in microstructure and properties, through the weld section (71). The composition variation is due to dilution effects - the root run may be diluted by as much as 70% by the parent plate, whereas the dilution of the capping run may be as low as 5%. Clearly, this will be most deleterious when the composition of the filler metal is significantly different to the parent plate - as exemplified by the case of cladded steels for either corrosion, wear or heat resistance (69,70). This dilution effect has been shown

to be one of the reasons for a decreased root run toughness in carbon-manganese steel welds (71,72). Strain aging has also been shown to cause a significant reduction in root run toughness in carbon-manganese steels. Clearly, dynamic strain aging can occur as the root run is re-heated by subsequent passes, and this causes an increase in the static yield strength, and a decrease in the resistance to cleavage (72,73).

In general, as the weld increases in size, different positions in the weld metal will experience greater differences in the amount of dilution by the parent plate, the number and rates of heating and cooling cycles, and the total strain. A study performed on the properties of equal double U butt welds (53) showed that the weld root had significantly lower fracture toughness, higher yield strength and higher hardness than the weld metal nearer the surface.

In the as-welded condition, the toughness of low alloy steel welds was seen to increase with increasing alloy content, particularly nickel, manganese and molybdenum; however, this increase in toughness with alloy content was shown to pass through a maximum value (71). Another study indicated, however, that additions of nickel or managanese were only beneficial at slow cooling rates (74). Both studies showed that, at high strength levels, decreasing the carbon content would result in improved toughness (71,74). Obviously, the strength and toughness of the weld metal is influenced by the type of flux used, since this influences the microstructure, as well as having a marked effect on the inclusion content of the weld. It was found that increasing the carbon, silicon, nitrogen and phosphorus contents of the flux material would decrease the weld metal toughness (75).

Most weld defects originate in the weld metal, or on the fusion line, but may easily grow into the heat affected zone. There are, in addition, certain defects which are almost exclusively situated in the heat affected zone, notably lamellar tearing, hydrogen or cold cracking and reheat cracking. Thus, it is often necessary to have some measure of the local toughness of the heat affected

zone (71,76,77). However, as with weld metals, the determination of heat affected zone toughness is a difficult problem. The first limitation arises due to the narrow width of the heat affected zone (77), and the significant variation in microstructure and hence properties within this zone, ranging from the "as-quenched" microstructure at the fusion line to the unaffected parent plate. Secondly, in a multipass weld, the heat-affected zone of the root run will be tempered by the subsequent runs, so that the microstructure and hence properties will vary with depth, as well as distance from the fusion line. Indeed, a study of the heat affected zone properties of ten different pipe-line steels (77) showed that the wide variation across each heat affected zone could not be predicted on the basis of microstructure or composition.

There are, however, a number of controls useful in improving the heat affected zone toughness (76), including: the use of low carbon and low carbon equivalent steels, using parent plate material which has a high toughness, and decreasing the niobium and vanadium content when the weld procedure has a high heat input. With regard to the first point, it is interesting to note that the conventional formula for the evaluation of carbon equivalent may not be appropriate for the more recently developed micro alloyed steels (77).

The process of welding leads to a compromise between a slow welding speed, so as to minimise metal disturbance, and a high welding speed so as to increase (or maintain) productivity (47). If the heat input can be minimised and the travel speed maximised, while maintaining a useful deposition rate, the width of the heat affected zone will decrease. Grain refinement is obviously beneficial to toughness, and this will be achieved if the weld runs in a multipass weld overlap.

However, with all these welding parameters taken into consideration, the fracture toughness of any welded structure will also depend on the rate of loading, the operating temperature and the thickness of the joint (45,78-80). Thus, any fracture toughness evaluation of a defective weldment must consider

all these service factors, as well as ensuring that the toughness is evaluated for the microstructure in the region of the defect.

4.1.2 The fabrication of specific weld defects

In order to be able to investigate the effect of weld defects on the fracture mode of weldments, reliable procedures for fabricating welds containing discrete defects have had to be developed (6,7,66). It is worth pointing out that the production of a welded joint containing a specific defect type is somewhat more difficult than fabricating a perfect weld. Indeed, the techniques developed are the antithesis of good welding practice, and it is therefore possible to draw comparisons between how to produce defects and how to avoid them.

Manual Metal Arc (MMA) and Submerged Arc (SA) welding techniques are prone to slag inclusions; these defects may be present at any position in a weld, either as small particles, or as a continuous line. A slag line may be produced at any position by leaving a gap in a weld run, and adjacent runs are laid so as to leave a small recess into which powdered slag can be poured. Tungsten Inert Gas (TIG) runs are laid on either side of the recess until a bridging run can be laid, at a low current, to cover the defect.

Porosity is possibly the most difficult defect to reliably fabricate in a weld, since subsequent passes may draw the porosity into the covering weld pool. Porosity can be introduced using Metal Inert Gas (MIG) welding by reducing the gas flow rate by 50%, or by using damp flux in the SA technique. Care must be taken with the covering passes in both cases.

It is possible to achieve lack of penetration in a closed butt weld using most welding techniques, simply by reducing the current. However, this may cause lack of root fusion, and lack of penetration defects can be made to order by machining the required defect size into the weld preparation (66). It is then not necessary to decrease the welding current, and proper fusion will be

achieved. The weld preparation used for this work was shown in Figure 2.4, and Figure 4.1 shows the fracture surface of some of the defective welds fabricated for this study: the wide range of defect sizes that were achieved illustrate the effectiveness of this technique.

Lack of fusion may be caused by the presence of heavy millscale on the plate surfaces which will prevent them from reaching the fusion temperature. Alternatively, incorrect manipulation of the welding rod or gun, or too low a current, will also result in lack of fusion. A further technique for inducing this defect is to use a high travel speed so that the weld metal is deposited on unmelted parent plate.

Solidification cracks, or hot cracks, will occur naturally when SA welding is used on a joint with a large depth-to-width ratio. Suitable parameters are 700A, 25V and 800mm/minute travel speed in a 6mm deep, 5mm wide joint preparation (7). The weld run should be at least 100mm long to ensure a 50mm defect in view of the time taken to reach the maximum welding speed. Heat affected zone cracking, cold cracking or hydrogen cracking can be promoted in a hardenable steel by welding with damp rutile electrodes, without using a preheat. Of all the defects discussed here, however, the manufacture of hydrogen cracking is probably the least reliable or controllable (7).

Thus it seems that, provided sufficient care is taken during welding, it is possible to artificially insert defects into a weld, in a controllable manner. As with good welding however, a certain amount of practice and experimentation is necessary, before a series of defective test plates can be reproducibly fabricated.

4.1.3 Stresses and strains induced during welding

A weld is essentially a small casting, where molten metal solidifies to form a joint between two adjacent members. The decrease in volume during the

solidification of a metal is well understood; for example in normal casting operations, allowances are made for this shrinkage (81,82). In a welding operation, however, these allowances cannot be made, and the contraction of the solidifying weld metal is constrained by the large masses of solid metal adjacent to it, thus giving rise to a self-equilibrating residual welding stress. Residual stress is possibly one of the least well understood entities of a component or structure as it enters its service life, and the magnitude of residual stresses can approach, or even exceed the yield strength of the material. For example, a 175mm diameter, 1250mm long shaft exploded into three pieces while lying, free of any external forces, on a laboratory floor (83). It is worth noting here that residual stresses can also arise from heat treatment (as exemplified by the quench cracking that can occur in alloyed steels), as well as machining operations (84).

In the case of a welded joint in a plate, there are lateral as well as longitudinal stresses due to weld metal shrinkage (84), as shown schematically in Figure 4.2. Figure 4.3 illustrates the changes in temperature and thermal stresses that arise during welding (85). Thus, the residual stresses are tensile in the weld metal, and compressive in the adjacent parent plate. This situation, which holds true for a single pass weld has added complexity for a multipass weld, when attempting to establish the nature and magnitude of the through-thickness residual stresses. These will depend on the welding method employed, the heat input, the number of passes and the pass sequence, plate thickness, joint constraint, included angle of the weld preparation, in addition to the parent plate and weld metal mechanical and thermal properties. It is common practice to stress-relieve a welded joint by heat-treatment; however, this is usually only effective in reducing the level of residual stresses to 10-25% of the (ambient temperature) yield stress (87).

If residual stresses can approach the material yield strength, then obviously they must be taken into account when performing any fitness-for-purpose assessment of defective welds. In the experimental justification for the design

curve in PD 6493, it was shown that the failure stress predictions for defective, as-welded plates only compared with those predicted for nominally residual stress-free plates when the assumption of yield strength magnitude residual stresses was made (88). However, the assumption of full-yield residual stresses may be overly conservative when applied to the full thickness, since residual stresses are by nature self-equilibrating, and hence the magnitude decays rapidly with distance from the surface (60,89). Furthermore, the transverse residual stresses are likely to be compressive at the mid-point of a thick joint, and thus defects situated there are less harmful than the same size of defect at or near the surface (88). In addition, the maximum residual stress magnitude, in a line transverse to the direction of welding, is unlikely to exceed the lowest yield strength of the various microstructures (weld metal, heat affected zone and parent plate) in that line (88).

Thus, it is clear that although residual stresses are significant, and should not be disregarded in an integrity assessment, the assumption that tensile, full yield residual stresses act throughout the thickness of a welded joint may be conservative. This then raises the question of how to measure the residual stress distribution in a weldment. Existing methods for measurement are limited in their capabilities and uncertain in their results (90), and many of these methods are destructive in that they rely on the measurement of deformations in a residually stressed body when a portion of that body is cut away. Hole-drilling and the layering technique are two examples of such dissection methods, although the former may be considered to be non-destructive since only a small hole is required and this may be subsequently repaired. Non-destructive testing methods such as X-ray diffraction, ultrasonics and photoelasticity can, in principle, be applied to every piece in a production lot, and are relatively rapid, compared to the destructive techniques (90).

However, the principal difficulty with such non-destructive methods is that they are all indirect, and measure some physical quantity influenced by the presence of residual stress. An example of this is the assessment of residual stress

magnitude using X-ray diffraction. This technique is based on measurements of lattice strains, or the changes in crystallographic lattice spacings, brought about by the residual stress. Another point of concern about this particular method is that the X-ray beam only interrogates a small volume of surface and near surface material, and measures both micro- and macro-stresses acting at that point.

Although in most cases, residual welding stresses are deleterious to the subsequent service performance of a structure or component, there are cases where they can be used to some advantage. An example of this is the current effort (see, for example, references 91 and 92), aimed at preventing intergrannular stress corrosion cracking (IGSCC) in type 304 stainless steel pipelines used in Boiling Water Reactors (BWR). The pipelines are formed by welding together the various pipe sections, and in this particular case, the IGSCC involves a complex interaction between material susceptibility, environment and the presence of a tensile residual welding stress. Since the environmental conditions exist inside the pipelines, by creating a compressive residual welding stress on the inner surface, the incidence of IGSCC has been much reduced. The compressive residual stresses are formed by a method known as heat sink welding (HSW) in which the pipe interior is cooled by water during all welds subsequent to the root pass (91,92).

Finally, it is worth noting that, as will be detailed in Chapter Five, to follow, residual welding stresses do not generally affect the fatigue performance of welded joints under tension-tension loading. Thus, the fatigue strength of an as-welded detail will not be improved by a heat-treatment stress relief, unless there is a significant compressive component in the loading cycle. This point will be addressed further in Chapter Five, to follow.

4.1.4 Summary

This Section has reviewed some of the problems associated with welding, and in

particular, the decreased toughness exhibited by the weld metal and heat affected zone regions in a weldment. While it is possible to obviate some of these difficulties, it will be essential that a fitness-for-purpose assessment of a defective weld in a safety critical component take account of the local microstructure around the defect. In order to assess the effect of weld defects on fracture behaviour, it is necessary to develop methods for the reliable and reproducible fabrication of defective welds and several such techniques have been outlined. Although welding residual stresses can reach yield stress magnitude in certain areas of a weld, these are self-equilibrating, and have been shown to decay rapidly with distance from the surface. Thus, the assumption of full tensile yield residual stresses throughout the joint thickness may be unnecessarily conservative. Residual stresses may be measured by destructive or non-destructive means, but there are problems associated with each type.

The remaining Sections in this Chapter detail the results obtained in the fracture mechanics assessments of defective welds, and compares these predictions to the experimental results obtained. In this test programme, the fracture toughness of the weld metal in the region of the defect was determined by conventional CTOD testing, and the lack of fusion defects were fabricating as described in Section 4.1.2. The effect of the welding residual stresses were established by performing some of the destructive tests on as-welded specimens, and the remainder on stress relieved specimens. In addition, the failure stress levels and defect criticalities calculated on the basis of the actual defect size in each test plate are compared to those calculated from ultrasonic defect size predictions, obtained in the two inspection programmes, as detailed in Chapter Two.

4.2 Experimental Details

As described in Section 4.1.3, welding residual stresses can affect fracture mechanics predictions of failure behaviour. However, in this work, it was

assumed that the residual stresses due to welding in these test plates were negligible since (a) the weld geometry was simple, with little restraint, (b) the test plate width (and therefore the weld length) was only 90 mm, and (c) the cappings runs had been machined off to facilitate the UT inspections. In order to test this hypothesis, twenty of the test plates were tested in the as-welded condition, and ten after a stress relief heat-treatment. The mechanical properties and fracture behaviour of the weld metal, heat affected zone and parent material were therefore established for both weld types, in both the as-welded and the stress-relieved condition (64,65). It should be pointed out, however, that the mechanical properties and fracture behaviour of the parent plate and heat-affected zone were not essential in the fracture mechanics assessment of these defects, which were all situated (by design) in the weld metal (66).

The recorded failure loads and defect parameters for the thirty test plates are shown in Table 4.1, from which it can be seen that there is no large, consistent difference between the failure loads recorded for the as-welded plates and those measured in the stress-relieved plates. If there had been residual stresses of any significant magnitude, then it is reasonable to assume that there would have been a much larger disparity than that observed.

The actual defect parameters (as measured from the fracture surface for each specimen) were used to calculate, from the graphs provided in the BS document (3), an effective defect parameter ($\bar{a}$) for the embedded defect. This effective defect parameter was then equated to the "maximum allowable" defect parameter, $\bar{a}_m$. The appropriate material properties were then used in conjunction with the Design Curve to extrapolate a failure stress level for this maximum allowable defect parameter. It should be noted here that, since the maximum allowable defect parameter is less, by a factor of about 2, than the critical defect parameter, $\bar{a}_{crit}$ (59), the failure stress level evaluated from the Design Curve for the maximum allowable flaw size should be correspondingly less than the stress required to cause failure.

Conditions for ligament stability were checked, and if required the defect was re-categorised as a surface defect, under the procedures set out in PD 6493, and a new failure stress calculated. The "PD 6493 predicted" failure load level calculated from this failure stress was then compared to the actual failure load recorded during the destructive testing. As can be seen from the effective defect parameter for each test plate (listed in Table 4.1), in most cases, the embedded defects were recategorised to surface defects.

The same procedure was used to calculate failure stress levels for the UT defects sized in each specimen in both the inspection programmes detailed in Chapter Two. For each test plate there was a minimum predicted failure stress (calculated from the "largest" defect) and a maximum predicted failure stress (calculated from the "smallest" defect). These were compared to the actual failure stress, as calculated from the measured defect, for each of the defective welds.

When assessing defect criticality using the CEGB R-6 method, it it will be recalled that it is necessary to calculate two parameters. Firstly, the elastic parameter, K_r, which is the ratio of the stress intensity of the defect under the applied loading condition to the plane strain fracture toughness (K_{Ic}) of the material in which the defect is sited. A plastic parameter, S_r, is then calculated from the ratio of the applied load to that load required for plastic collapse. As described in Chapter Three, these two parameters are then used as coordinates to define a point on the "Failure Assessment Diagram"; depending on the location of the point relative to the failure assessment line, the defect is either classed as safe or unsafe. In this work, the stress intensity was calculated using the method for LEFM conditions in PD 6493 (3), and the plastic collapse load was evaluated as shown in Chapter Three.

As pointed out in Section 3.1.4, the original R-6 Failure Assessment Line was

established for an ideal material in which strain hardening did not occur. Clearly then, this Failure Assessment Line will be somewhat conservative when applied to real engineering materials. Therefore, the first step of the R-6 analysis in this study was to use the actual defect parameters (as measured from the fracture surface in each specimen) and failure loads as input in the assessment, and establish the Failure Assessment Line for these particular materials. Having established this experimental failure condition, the UT predictions of the defect sizes in each test plate could be used as input data in the analysis, and the predicted defect criticalities compared to the actual defect criticalities and the experimental Failure Assessment Line.

4.3 Results and Discussion

4.3.1 The BS PD 6493 Approach.

As described in the preceding Section, the failure loads were recorded for each specimen, and these were compared to the failure load calculated from the PD 6493-predicted failure stress. These results are shown schematically in Figure 4.4, and it is clear from this figure that, without exception, the recorded failure loads exceed those calculated via the Design Curve.

As outlined above, this approach (3) is known to have a "built-in" factor of conservatism (59), and therefore the ratio of the applied failure load to that predicted via the Design Curve was calculated for each specimen. (This load factor is also indicated in Figure 4.4). The average load factor of each specimen set was calculated to be 1,79 for the as-welded MMA test plates, 1,42 for the as-welded SA plates and 2,33 and 1,46 for the stress relieved MMA and SA plates respectively. Thus, for the thirty defective plates, and four weld metal types, the average factor of conservatism in the predicted failure loads is 1,70. This spread in the results is to be expected, since the different weld metals have different toughnesses and different stress-strain behaviour and will therefore exhibit different "defect tolerances". Additionally, the failure

stress or strain obtained from the Design Curve is not a linear function of the defect parameter. However, these results are consistent with other published work (59).

One point worth noting is that the Design Curve in the BS approach requires, as material input data, a "critical" value of the CTOD toughness. In this work the CTOD at maximum load was used throughout, since the failure loads in the destructive testing were defined as the maximum load sustained by each specimen. (The Welding Institute have indicated that the initiation CTOD is, for general usage, unnecessarily conservative (67)). If, for instance, the initiation CTOD had been used in this evaluation, the failure loads calculated from the Design Curve would have been correspondingly lower. Thus, the factor of safety evaluated for the PD 6493 failure loads would have been greater than 2. However, it must be reiterated that a number of assumptions were made when evaluating the failure stress from the PD 6493 predicted failure strain ratio, and although this was shown, by means of a theoretical sensitivity analysis (see reference 94 and Chapter Three) to be a reasonable engineering solution, it cannot be regarded as completely rigorous, and thus the actual factor of conservatism may in fact be higher than the values shown above.

The failure stress calculated from the actual defect parameters was then compared to the failure stress predicted from the UT defect sizes. These results are shown schematically in Figure 4.5 for the as-welded MMA specimens, the as-welded SA specimens and the stress relieved test plates. As can be seen from this figure, there is a significant difference between the minimum and maximum predicted failure stresses (defined here as the "stress range"). In addition, in nine of the thirty specimens, the minimum predicted failure stress was greater than the actual failure stress. In other words, if these (minimum) UT defect size predictions had been used to establish maximum working stresses for these welds, these could have resulted in unanticipated failures.

The average stress ranges in the specimen sets were calculated to be 145 MPa and

197 MPa for the as-welded MMA and SA weldments and 313 MPa and 188 MPa for the stress relieved MMA and SA weldments respectively. These stress ranges are less than half of the material yield stress in each case, whereas the average differences between the maximum and minimum effective defect parameters were 17,5 mm, 20,9 mm, 20,4 mm, and 21,9 mm for the as-welded and stress-relieved MMA and SA specimen sets respectively. These average differences are of the same order as (and in some cases greater than) the actual effective defect parameter for each specimen (these are listed in Table 4.1). However, the average failure stresses calculated for the actual defects in the four specimen sets were 545 MPa, 525 MPa, 388 MPa and 456 MPa for the MMA and SA as-welded and stress-relieved specimens respectively. Thus, it can be seen that although the differences observed in the defect parameters evaluated from UT size predictions are of the same order as the actual defect parameters, the corresponding differences in the UT failure stress predictions (the stress range) are less than the actual failure stresses. This therefore indicates some tolerance in the PD 6493 approach (for these particular weld metals) to the very significant variations observed in UT predictions of defect sizes. It also shows that the stress-relieved MMA material is most affected by the inaccuracies in the defect sizing, since this specimen set recorded the largest average stress range, in comparison to the average of the failure stress predicted from the actual defect in each of the five specimens. This is consistent with the results obtained in the theoretical sensitivity analysis, detailed in the preceding Chapter.

It will be recalled that the ten testplates that were tested in the stress-relieved condition were examined in both "round-robin" UT inspection programmes. Thus the same analysis could be used to calculate the PD 6493 failure stresses from the defect sizes predicted in the second inspection programme. The results are also shown schematically in Figure 4.5, ie. comparing the minimum and maximum failure stresses obtained from the predicted defect sizes to that calculated for the actual defect in each of the ten test plates. The improved accuracy in defect sizing is reflected by the lower stress

range for each of the specimens, which was averaged at 33 MPa for the five MMA test plates (yield stress 666 MPa), and 81 MPa for the five SA test plates (yield stress 599 MPa). This improved defect sizing is also reflected by the difference in the minimum and maximum effective defect parameters, which were averaged at 3,6 mm and 5,5 mm for the five MMA and five SA specimens respectively. These average differences correspond to 15.5% and 24 % of the average effective defect parameters calculated for the actual defect sizes in the respective specimen sets.

The lower average stress range for the stress-relieved MMA set appears to be at variance with the trend observed in the results obtained from the initial UT inspection where it was seen that this material was the most affected by inaccuracies in defect size predictions. However, the Design Curve is not linear, and thus the lower stress range calculated for the stress-relieved MMA specimens is due to the smaller difference between the minimum and maximum effective defect parameters.

4.3.2 The CEGB R-6 method

Initially, the actual defect sizes and the applied (i.e. actual) failure loads were used as input data, and the Failure Assessment Diagrams for the four weld types are shown in Figures 4.6 (a) and (b). It can be seen that the R-6 Failure Assessment Line is somewhat conservative in all cases. Thus, a postulated Failure Assessment Line, based on experimental results, has been drawn in to represent what is thought to be critical conditions for these particular specimens. It is apparent from these Figures that the two as-welded specimen sets can be defined by a single failure line, as can the two stress-relieved specimen sets. The theoretical sensitivity analysis performed on these weld metals (Chapter Three) indicated that the stress-relieved MMA weld metal was the most defect tolerant, and thus could be expected to show a different failure line, relative to the other three weld metals. This should not be seen as questioning the validity of the sensitivity analysis, however, since the

sensitivity analysis was a purely theoretical excercise, which was carried out for a reference defect in a constant plate section, under a constant applied bending load. As described in Chapter Three, each defect parameter was then varied, whilst the other two were kept constant, in order to assess the sensitivity of the analyses used to each parameter. Thus, for the actual test plates, where all defect parameters (as well as plate dimensions and applied loads) were variable, it can be expected that the locus of these failure assessment points may be somewhat different to that obtained for the same materials in the sensitivity analyses.

It should also be noted that the Failure Assessment Lines calculated on the basis of material strain hardening characteristics and shown in Figure 4.7 (61) are still somewhat conservative when compared to these experimental results. As shown in this Figure, for the four materials under consideration here, the ratio of Tensile Strength to Yield Stress is 1,2 for the as-welded and stress relieved MMA and the stress-relieved SA weld metals, and 1,1 for the as-welded SA weld metal. It is considered that this apparent conservatism is due to the method used to calculate the plastic collapse load for these specimens.

Having established the Failure Assessment Line for each weld type, the UT predictions of defect sizes were used to calculate the relevant K_r and S_r parameter for each predicted defect in each test plate. The latter was calculated from the ratio of the applied failure load to the plastic collapse load calculated on the basis of the predicted defect size. The stress intensity (K_I) was also calculated using the predicted defect parameters. Thus, since failure did indeed occur in all cases, the UT predictions of defect size should, ideally, describe a point in the critical region of the Failure Assessment Diagram.

In actuality, however, the wide range of UT predictions of defect sizes obtained in the initial test programme was reflected in the wide range of defect criticalities, as evidenced in Figure 4.8 and 4.9 which show the results

Author Boothroyd Colin Allistair
Name of thesis Fracture Mechanics Analyses Of Static And Dynamic Failures Associated With Welding. 1986

PUBLISHER:
University of the Witwatersrand, Johannesburg
©2013

LEGAL NOTICES:

Copyright Notice: All materials on the University of the Witwatersrand, Johannesburg Library website are protected by South African copyright law and may not be distributed, transmitted, displayed, or otherwise published in any format, without the prior written permission of the copyright owner.

Disclaimer and Terms of Use: Provided that you maintain all copyright and other notices contained therein, you may download material (one machine readable copy and one print copy per page) for your personal and/or educational non-commercial use only.

The University of the Witwatersrand, Johannesburg, is not responsible for any errors or omissions and excludes any and all liability for any errors in or omissions from the information on the Library website.